Quantitative proteomics combined with network pharmacology analysis unveils the biological basis of Schisandrin B in treating diabetic nephropathy

Jianying Song[1, a], Bo Zhang[1, b, c], Xudong Lyu[1, a], Huiping Zhang[d], Wenbo Cheng[*e], Peiyuan Liu[*a], Jun Kang[*a]

a. School of Life Sciences, Tianjin University, 92 Weijin Road, Nankai District, Tianjin 300072, People's Republic of China

b. Institute for TCM-X, MOE Key Laboratory of Bioinformatics, Bioinformatics Division, BNRist, Department of Automation, Tsinghua University, Beijing 100084, China

c. Beijing Intelligent Medicine and Network Pharmacology Co., Ltd, Beijng 100020, China

d. Shanghai Applied Protein Technology Co., Ltd., 58 Yuanmei Road, Shanghai 200233, People's Republic of China

e. Tianjin Key Laboratory of Medical Mass Spectrometry for Accurate Diagnosis, Tianjin 300399, People's Republic of China

Jianying Song and Bo Zhang contributed equally to this work. Author order was determined on the basis of seniority.

Address correspondence to Jun Kang, jun.kang@tju.edu.cn; or Peiyuan Liu, peiyuan.liu@tju.edu.cn; or Wenbo Cheng, chengwb@sibet.ac.cn.

Running title: Biological basis of Schisandrin B to treat diabetic nephropathy

Abstract

***Background*:** Diabetic nephropathy (DN) is a major complication of diabetes. Schisandrin B (Sch) is a natural pharmaceutical monomer that was shown to prevent

kidney damage caused by diabetes and restore its function. However, there is still a lack of comprehensive and systematic understanding of the mechanism of Sch treatment in DN.

***Objective*:** We aim to provide a systematic overview of the mechanisms of Sch in multiple pathways to treat DN in rats.

***Methods*:** Streptozocin was used to build a DN rat model, which was further treated with Sch. The possible mechanism of Sch protective effects against DN was predicted using network pharmacology and was verified by quantitative proteomics analysis.

***Results*:** High dose Sch treatment significantly downregulated fasting blood glucose, creatinine, blood urea nitrogen, and urinary protein levels and reduced collagen deposition in the glomeruli and tubule-interstitium of DN rats. The activities of superoxide dismutase (SOD) and plasma glutathione peroxidase (GSH-Px) in the kidney of DN rats significantly increased with Sch treatment. In addition, the levels of IL-6, IL-1β, and TNF-α were significantly reduced in DN rats treated with Sch. 11 proteins that target both Sch and DN were enriched in pathways such as MAPK signaling, PI3K-Akt signaling, renal cell carcinoma, gap junction, endocrine resistance, and TNF signaling. Furthermore, quantitative proteomics showed that Xaf1 was downregulated in the model vs. control group and upregulated in the Sch-treated vs. model group. Five proteins, Crb3, Tspan4, Wdr45, Zfp512, and Tmigd1, were found to be upregulated in the model vs. control group and downregulated in the Sch vs. model group. Three intersected proteins between the network pharmacology prediction and proteomics results, Crb3, Xaf1, and Tspan4, were identified.

***Conclusion*:** Sch functions by relieving oxidative stress and the inflammatory response by regulating Crb3, Xaf1, and Tspan4 protein expression levels to treat DN disease.

Keywords: Diabetic nephropathy; Schisandrin B; Crb3; Tspan4; Xaf1.

1. INTRODUCTION

Diabetic nephropathy (DN) is one of the major complications of diabetes and a major

cause of end-stage renal failure, with about 30% of diabetic patients deteriorating into DN [1]. Early symptoms include increased glomerular filtration capacity and the appearance of microalbumin in urine. If not treated, glomerular atrophy, basement membrane thickening, and extracellular matrix accumulation may lead to chronic renal insufficiency [2]. Deteriorating even further into clinical proteinuria, the renal function will experience a sharp decline that gives rise to end-stage renal failure [3], seriously affecting the quality of life of patients. At present, the treatment methods for DN mainly encompass controlling blood glucose levels and regulating lipid metabolism with antihypertensive drugs [4, 5] and vitamins [6]. However, existing treatment methods have failed to completely prevent the deterioration of DN [7]. Therefore, new drugs or treatments that could improve the renal function of DN patients and alleviate the progression of the disease have attracted much attention.

The immune and inflammatory mechanisms play a pivotal role in the development of DN, which is considered to be a chronic inflammatory disease [8]. Several types of cells, such as monocytes, macrophages, and lymphocytes, as well as chemokines and cytokines, are involved in this process [9, 10]. Among them, it is well known that interleukin 6 (IL-6), interleukin 1 beta (IL-1β), and tumor necrosis factor-alpha (TNF-α) are related to the progression of DN, due to their ability to induce kidney cells to produce various chemokines, triggering the next round of inflammatory responses [11, 12]. Diabetic patients often suffer from obesity, insulin resistance, and increased oxidative stress. It was also found in diabetic patients that the levels of heat shock protein 60 and free fatty acids were increased, the expression of TLR4 was significantly increased, and the downstream molecule NF-κB translocated into the nucleus. This activated the TLR4/NF-κB inflammatory signal transduction pathway, which promoted the transcription of downstream inflammation-related genes, inducing the production of a large number of cytokines and inflammatory mediators, which further led to renal inflammatory damage [13, 14].

Schisandrin B (Sch) is a natural active lignin compound extracted and isolated from the

traditional Chinese medicine *Schisandra chinensis*. Sch was shown to exhibit significant antioxidant, anti-inflammatory, and anti-apoptotic effects and to support the health of organs such as the heart [15-17], brain [18, 19], liver [20], and kidney [21]. Sch was shown to be involved in the renal protection of type 2 DN rats by regulating the HMGB1/TLR4 signaling pathway [22]. Sch improved renal function by intervening in the Nrf2/ARE signaling pathway, thus exerting a protective effect on rats with nephrotic syndrome [23]. Sch also alleviated hyperglycemia-induced renal injury by suppressing excessive inflammation and oxidative stress through maintenance of urine creatinine and albumin levels in a diabetic mouse model [24]. Despite the exceptional curative potential and effects on DN, the overall systematic understanding of the molecular mechanism of Sch in the treatment of DN disease is still lacking.

As the globalization movement and digitalization become the mainstream of modern research, the combination of bioinformatics with traditional experimental methods has received much attention and enthusiasm. Network pharmacology is a new discipline based on the theory of system biology, which analyzes a network of biological systems and selects specific signal nodes for molecular design of multiple drug targets [25, 26]. Traditional Chinese medicine (TCM) network pharmacology, which is firstly proposed by Li [27, 28], provide a new systematic way to understanding TCM and is widely used in exploring mechanism underlying natural products [29, 30]. It is a useful and comprehensive tool to elucidate complicated relationships among drugs, gene targets, and diseases based on building a network. Network pharmacology emphasizes the regulation of signaling pathways in multiple ways to improve the therapeutic effect of drugs and reduce side effects, so as to improve the success rate of clinical trials of new drugs and reduce the cost of drug research [31-35].

In this article, high-fat feed combined with streptozocin (STZ) injection was used to establish a DN rat model. The effect of Sch treatment on differential expression of proteins in the kidneys of the DN rats was explored and clarified by network

pharmacology and proteomics for a systematic and comprehensive understanding of the molecular mechanism of Sch treatment of DN disease (Scheme 1).

2. MATERIALS AND METHODS

2.1. Reagents

Sch was purchased from Shanghai Yuanye Bio-Technology Co., Ltd. (61281-37-6, Shanghai, China). Irbesartan was purchased from Lunan Beite Pharmaceutical Co., Ltd. (Batch No. 36160901, specification: 40 mg/tablet, Shandong, China).

2.2. Modeling

Fifty healthy specific-pathogen free male Sprague-Dawley rats, 6–8 weeks old, weighing 200±20 g, were provided by Beijing HFK Bioscience Co., Ltd. (quality certificate No. 110322210100331916). The feeding environment was maintained at 25±2°C, the relative humidity was 50±15%, there was a 12-h light and dark cycle, and the rats had free access to food and water. The experimental conditions were improved and optimized based on Azushima's research [36]. The experiment was approved by the Ethics Committee of Tianjin University.

After 1 week of adaptive feeding, 10 rats were randomly chosen as the negative control group, and the other 40 rats were fed a high sugar and high fat diet (10% lard, 20% sucrose, 2.5% cholesterol, and 67.5% conventional diet). Intraperitoneal injection of STZ at 30 mg/kg [1% STZ solution prepared with 0.1 mmol/L citric acid-sodium citrate buffer (pH 4.4)] was performed at the end of the 7th week. After 72 h, blood samples from the tail vein were randomly collected to test blood glucose content. The modeling of diabetic rats was regarded as successful if the blood glucose concentration exceeded 16.7 mmol/L. Diabetic rats were fed for another week, and 24 h urine was collected using metabolic cages after 1 week to measure urine protein content. The DN animal model was established with the standard of a blood glucose concentration exceeding 16.7 mmol/L, positive urine glucose, and positive urine protein. During modeling, the

weight of the rats in each group was recorded every 2 weeks.

Successfully modeled rats were randomly divided into a model group, a positive control group, an Sch low dose group, and an Sch high dose group, with 10 rats in each group. The positive control group was administered irbesartan at 30 mg/kg [37], the Sch low dose group at 20 mg/kg, and the Sch high dose group at 40 mg/kg. The negative control group and model group were administered the same volume of distilled water by intragastric administration for 4 continuous weeks. During the experiment, the rats were fed a standard diet and had free access to drinking water. Food was withheld for 12 h every Saturday night to collect blood from the tail vein to measure the fasting blood glucose at 8:00 a.m. on Sunday.

2.3. Biochemical index analysis

Four weeks after the Sch intervention, 24 h urine collections for each rat from each group were performed by using metabolic cages. The urine was centrifuged at 4000 g for 10 min, and the 24 h urinary albumin concentration was measured. The rats were anesthetized by an intraperitoneal injection of 50 mg/kg pentobarbital sodium, and the inner canthus blood was collected. The collected blood was centrifuged at 3000 r/min for 15 min, and serum was collected. The serum levels of serum creatinine and blood urea nitrogen (BUN) were determined by an automatic biochemical analyzer.

After blood collection, the rats were killed using cervical dislocation. Kidneys were removed immediately, and part of the rat kidney tissue was extracted, washed with pre-cooled phosphate-buffered saline three times, homogenized at a low temperature after cutting, centrifuged at 16,000 g for 10 min, and the supernatant was collected. The activities of superoxide dismutase (SOD) and plasma glutathione peroxidase (GSH-Px) and malondialdehyde (MDA) levels related to oxidative stress were measured according to the steps described in the kit.

175 **2.4. ELISA**

176 The levels of IL-6, IL-1β, and TNF-α in the renal tissue homogenate were determined
177 by ELISA. First, 100 μL of IL-6, IL-1β, and TNF-α captured antibodies was added to
178 ELISA plates and incubated overnight at room temperature. The plates were washed
179 and blocked for 1 h, then washed, and 100 μL of rat kidney tissue homogenate was
180 added. Three replicates were used for each sample. The plates were incubated at room
181 temperature for 3 h and washed afterwards. The plates were incubated with the
182 corresponding enzyme-conjugate secondary antibody for 30 min and washed
183 afterwards. After adding the chromogenic solution, the absorbance was read at a
184 wavelength of 405 nm, and the concentrations of IL-6, IL-1β, and TNF-α were
185 calculated.

186

187 **2.5. Histopathological staining of the kidney**

188 The renal tissues of rats in each group were fixed with a 10% formalin solution for 24
189 h, washed with water for 20 min, dehydrated with an alcohol gradient, made transparent
190 with xylene, embedded in paraffin, and sectioned into 5-μm slices for hematoxylin and
191 eosin (HE) staining, Masson staining, and Sirius red staining in order to observe the
192 basic pathological changes of the renal tissues in each group under a microscope.

193

194 **2.6. Drug and disease target prediction**

195 The Sch target proteins were predicted using the ChEMBL (www.ebi.ac.uk) and CTD
196 databases (ctdbase.org/). The screening standard was as follows: confidence was 90%
197 for ChEMBL, and interaction was "increases, decreases, or affects" for the CTD
198 database. The DN disease targets were predicted using the GeneCards
199 (www.genecards.org) and TCMSP (old.tcmsp-e.com) databases.

200

201 **2.7. Quantitative proteomics**

202 **2.7.1. Protein extraction and digestion**

203 Highly abundant protein was first removed from the samples, and then, SDT buffer (4%

204 SDS, 100 mM Tris-HCl, 1 mM DTT, pH 7.6) was used for sample lysis and protein
205 extraction. The amount of protein was quantified using a BCA Protein Assay kit (Bio-
206 Rad, USA). An appropriate amount of protein was removed from each sample and
207 digested by trypsin according to the filter-aided sample preparation procedure [38]. The
208 digested peptides of each sample were desalted on C18 cartridges [Empore™ SPE
209 Cartridges C18 (standard density), bed I.D. 7 mm, volume 3 mL, Sigma], concentrated
210 by vacuum centrifugation, reconstituted in 40 μL of 0.1% (v/v) formic acid, and
211 measured at OD_{280}.
212
213 **2.7.2. Tandem mass tag labeling**
214 Each sample containing a 100 μg peptide mixture was labeled using tandem mass tag
215 reagent according to the manufacturer's instructions (Thermo Scientific). The negative
216 control group samples were labeled C1, C2, and C3, the model group samples were
217 labeled M1, M2, and M3, and the Sch-treated model group samples were labeled S1,
218 S2, and S3, so that each group had three biological replicates, for nine samples in total.
219
220 **2.7.3. Grading**
221 For RP grading, the labeled peptides of each group were mixed in equal amounts and
222 fractionated by a high pH reversed-phase peptide fractionation kit (Thermo Scientific).
223 The column was first balanced by acetonitrile and 0.1% trifluoroacetic acid (TFA), then
224 the mixed labeled peptide samples were loaded and pure water was added, followed by
225 low-speed centrifugation for desalting. Finally, the column-bound peptides were
226 gradient eluted by a high pH gradient of an acetonitrile solution with successively
227 increasing concentrations. Each eluted peptide sample was vacuum-dried and
228 lyophilized with 12 μL 0.1% FA, and the concentration of the peptides was determined
229 by the OD_{280}.
230
231 For SCX grading, the labeled peptides of each group were mixed and graded using an
232 AKTA Purifier 100. Buffer A was 10 mM KH_2PO_4, and 25% ACN, pH 3.0, and buffer

B was 10 mM KH_2PO_4, 500 mM KCl, and 25% ACN, pH 3.0. The chromatographic column was balanced with buffer A, and samples were added into the chromatographic column for separation at a flow rate of 1 mL/min. The gradient of the liquid phase was as follows: the gradient of buffer B was 0% for 25 min, and then, the linear gradient of buffer B increased from 0% to 10% from 25 to 32 min; then, it increased 10%–20% from 32 to 42 min; then, it increased 20%–45% from 42 to 47 min; then, it increased 45%–100% from 47 to 52 min and then remained at 100% from 52 to 60 min. After 60 min, buffer B was reset to 0%. The absorbance value at 214 nm was monitored during elution. Eluted components were collected at 1 min intervals and lyophilized with C18 cartridges for desalting.

2.7.4. LC-MS/MS analysis

Each sample was separated by an HPLC liquid system, Easy nLC, at a nanoliter flow rate. Buffer A was a 0.1% formic acid aqueous solution, and buffer B was a 0.1% formic acid acetonitrile aqueous solution (the acetonitrile solution was 84%). The chromatographic column was balanced with 95% buffer A, and the samples were loaded onto the loading column by an automatic sampler (Thermo Scientific Acclaim PepMap100, 100 μm × 2 cm, nanoViper C18). The separation was performed on a Thermo Scientific EASY Column (10 cm, ID 75 μm, particle size 3 μm, C18-A2) at a flow rate of 300 nL/min. The samples were separated by chromatography and analyzed by a Q-EXactive mass spectrometer. The detection method was positive ion, the scanning range of the parent ion was 300–1800 m/z, the resolution of the first-level mass spectrometry was 70,000 at 200 m/z, the automatic gain control target was 1E6, the maximum IT was 50 ms, and the dynamic exclusion time was 60.0 s. The mass charge ratios of peptides and peptide fragments were collected as follows: twenty fragment profiles (MS2 scan) were collected after each scan. The MS2 activation type was HCD, and the isolation window was 2 m/z. The secondary mass spectrometry resolution was 17,500 at 200 m/z. The normalized collision energy was 30 eV, and the underfill was 0.1%.

262

263 **2.7.5. Identification and quantitation of proteins**

264 The MS raw data for each sample were searched using the MASCOT engine (Matrix
265 Science, London, UK; version 2.2) embedded in Proteome Discoverer 1.4 software for
266 identification and quantitative analysis.

267

268 **2.8. Statistical method**

269 The statistical software SPSS 20.0 was used to analyze the experimental data. Data
270 were expressed as mean ± standard deviation (x ± s), a *t* test was applied for
271 comparisons between two groups, and one-way analysis of variance (ANOVA) was
272 applied for comparisons between multiple groups. $P < 0.05$ was considered as a
273 statistically significant difference.

274

275 **3. RESULTS**

276 **3.1. Sch effects on blood glucose, renal function, and pathological manifestations**
277 **in DN rats**

278 After treating DN rats with Sch, the body weight of the model group decreased
279 significantly ($P < 0.01$) compared to the negative control group, and the body weight
280 of the positive control group, Sch low dose group, and Sch high dose group increased
281 significantly ($P < 0.01$, $P < 0.05$, and $P < 0.001$, respectively) compared to the model
282 group (Figure 1A).

283

284 The concentrations of fasting blood glucose were above 16.7 mmol/L in all rats 72 h
285 after STZ injection. After 4 weeks of Sch feeding, the fasting blood glucose in the Sch
286 low dose group and Sch high dose group decreased significantly ($P < 0.05$ and $P <$
287 0.001, respectively, Figure 1B) compared to the model group. Renal function tests
288 revealed that the creatinine, BUN, and 24 h urinary protein levels in the model group
289 all increased significantly ($P < 0.001$, $P < 0.01$, and $P < 0.001$, respectively) compared
290 to the negative control group. Irbesartan and high dose Sch treatments significantly

291 reduced the levels of creatinine ($P < 0.05$ and $P < 0.05$, respectively) (Figure 1C), BUN
292 ($P < 0.001$ and $P < 0.001$, respectively) (Figure 1D), and 24 h urinary protein ($P < 0.001$
293 and $P < 0.001$, respectively) (Figure 1E) in DN rats, while low-dose Sch treatment had
294 no significant effect.
295
296 HE staining demonstrated that the glomerulus and renal tubules in the negative control
297 group were normal, and no proliferation of mesangial cells or the mesangial matrix or
298 inflammatory cell infiltration was observed. The model group showed focal
299 degeneration and atrophy of renal tubules, slight thickening of the glomerular basement
300 membrane, hyperplasia of mesangial cells, and steatosis of glomerular and renal tubules.
301 Compared with the model group, the lesions in the experimental group were reduced,
302 and the improvement was more obvious in the positive control group and Sch high dose
303 group (Figure 2A). After Masson staining, collagen appeared blue under a light
304 microscope. The glomerulus and renal tubules of rats in the negative control group were
305 normal, and collagen expression did not increase, while collagen hyperplasia was
306 observed in the mesangial area and basement membrane, and renal tubules were dilated
307 in the model group. After Sch intervention, collagen deposition in the glomerulus and
308 intertubular tissues of DN rats was significantly reduced (Figure 2B). Sirius red staining
309 was used to indicate collagen deposition in the renal interstitium and vascular wall. The
310 study showed that the glomerular arteriole wall of the model group was thickened, but
311 the thickening degree of the high dose Sch treated group was weakened (Figure 2C).
312
313 **3.2. Sch effects on oxidative stress and inflammatory factors in DN rats**
314 The effects of Sch on oxidative stress in DN rats were further explored by measuring
315 the SOD, MDA, and GSH-Px levels in the renal tissue homogenates of rats in each
316 group. ELISA was used to determine the levels of pro-inflammatory factors IL-6, IL-
317 1β, and TNF-α in the renal tissue homogenates of the rats in each group to evaluate the
318 effect of Sch on the inflammatory response. When compared to the negative control
319 group, the activities of SOD and GSH-Px in the renal tissue homogenate of the model

group showed a significant decline ($P < 0.001$), while the level of MDA showed a significant surge ($P < 0.001$). Irbesartan and high dose Sch intervention promoted the activities of SOD ($P < 0.001$ and $P < 0.001$, respectively) (Figure 3A) and GSH-Px ($P < 0.001$ and $P < 0.001$, respectively) (Figure 3A and C) but diminished the level of MDA ($P < 0.01$ and $P < 0.05$, respectively) (Figure 3B) in renal cells. ELISA results showed that the serum levels of the pro-inflammatory factors IL-6, IL-1β, and TNF-α in the model group significantly increased (all $P < 0.01$) compared to the negative control group. In addition, irbesartan and high dose Sch intervention significantly reduced the serum levels of IL-6, IL-1β, and TNF-α in DN rats (Figure 3D). In summary, the results taken together substantiated that Sch produced a therapeutic effect in DN rats, especially at a high dose, and therefore, the high dose was selected for subsequent experiments.

3.3. Network pharmacology analysis

With the aim of uncovering the effects of Sch on gene expression in the renal tissues of DN rats, network pharmacological prediction was used to elucidate the molecular mechanism of Sch in the treatment of DN, according to the Network Pharmacology Evaluation Method Guidance [39]. First, the ChEMBL and CTD databases were used to predict possible targets of Sch, and 34 target proteins were identified. According to the GeneCards and TCMSP databases, there were 3424 target proteins affected by DN disease. Eleven proteins, including XIAP associated factor 1 (XAF1), glutamic-pyruvic transaminase (GPT), glutamate-cysteine ligase catalytic subunit (GCLC), glutathione-disulfide reductase (GSR), FMS-related receptor tyrosine kinase 1 (FLT1), mitogen-activated protein kinase 1 (MAPK1), Crumbs cell polarity complex component 3 (Crb3), tetraspanin 4 (Tspan4), checkpoint kinase 1 (CHEK1), and mitogen-activated protein kinase 3 (MAPK3), and nuclear receptor subfamily 1 group I member 2 (NR1I2) were identified as targets of both Sch and DN disease by a Venn diagram (Figure 4A; Supplemental Table S1). GO analysis of the 11 proteins revealed that the top three biological processes in terms of enrichment were aging, apoptotic process, and protein

349 phosphorylation (Figure 4B); the top three cell components in terms of enrichment were
350 nucleus, mitochondrion, and nucleoplasm (Figure 4C); and the top three molecular
351 functions in terms of enrichment were ATP binding, MAP kinase kinase activity, and
352 MAP kinase activity (Figure 4D). KEGG pathway analysis was conducted with the
353 purpose of discovering the enriched pathways of the 11 target genes. The results showed
354 that the genes were enriched in the MAPK signaling pathway, PI3K-Akt signaling
355 pathway, renal cell carcinoma, gap junction, endocrine resistance, and TNF signaling
356 pathway (Figure 4E). Finally, a "bioactive-protein-pathways" interaction network was
357 built to capture the relationship network between Sch, the target genes, and the related
358 pathways (Figure 4F).
359
360 **3.4. Quantitative proteomics analysis**
361 With the aim to detect protein expression changes caused by Sch in the kidneys of DN
362 rats, proteomic sequencing was performed on the negative control group, model group,
363 and Sch high dose group. The statistical results obtained of the spectrogram number,
364 identified peptide number, and identified protein number are shown in Supplemental
365 Figure 1. Using a screening standard of a fold change greater than 1.2 or lower than
366 0.83, as well as a P value < 0.05 *(t* test), the significantly differentially expressed
367 proteins were effectively selected and separated into each group, indicating that the
368 differentially expressed proteins could represent the effects of biological treatment on
369 samples. The raw data of the quantitative proteomics with differentially expressed
370 proteins marked with highlighting are presented in Supplemental Tables S2–S4.
371
372 First, we compared the overall differentially expressed proteins between the model vs.
373 control group and between the Sch-treated vs. model group (Figure 5A and 5B). The
374 differentially expressed protein, Xaf1, was found downregulated (0.80) in the model vs.
375 control group and upregulated (1.24) in the Sch-treated vs. model group. Furthermore,
376 five proteins were found upregulated in the model vs. control group and downregulated
377 in the Sch-treated vs. model group: Crb3 (1.24; 0.80), Tspan4 (1.23; 0.77), WD repeat

378 domain 45 (Wdr45) (1.36; 0.72), zinc finger protein 512 (Zfp512) (1.36; 0.73), and
379 transmembrane and immunoglobulin domain containing 1 (Tmigd1) (1.26; 0.82). These
380 proteins were considered as the possible targets of Sch in treating DN disease.
381
382 Next, we analyzed the differentially expressed proteins in the Sch-treated vs. model
383 group (Figure 5C). GO term analysis was conducted to find the differentially expressed
384 proteins. Fisher's exact test was conducted to find the significant difference between
385 the two and the functional categories of differentially expressed protein enrichment (*P*
386 value < 0.05). The column diagram showed the general results of GO (Figure 5D), and
387 the bubble diagram showed the enrichment of the three GO terms: biological process,
388 cell component, and molecular function (Figure 5E–5G). The results showed that most
389 genes were enriched in the following biological processes: cytokine biosynthetic
390 process, cytokine metabolic process, mucopolysaccharide metabolic process,
391 regulation of cytokine biosynthetic process, positive regulation of cytokine biosynthetic
392 process, and proteoglycan metabolic process. Additionally, the following molecular
393 functions underwent significant alterations: cGMP−dependent protein kinase activity,
394 acetylcholine receptor binding, TIR domain binding, mismatch repair complex binding,
395 and DNA polymerase processivity factor activity.
396
397 Protein coordination should be emphasized to gain a systematic and comprehensive
398 understanding of a biological process, the mechanisms of disease occurrence, and the
399 mechanisms of drug action. The Kyoto Encyclopedia of Genes and Genomes pathway
400 (KEGG) database was utilized to analyze and annotate proteins. As shown in Figure
401 5H, among the differentially expressed protein pathways, the main enriched pathways
402 were MAPK signaling, NF-κB signaling, Toll-like receptor signaling, NOD-like
403 receptor signaling, gap junction, mismatch repair, regulation of lipolysis in adipocytes,
404 and renin secretion (Figure 5H).
405
406 **3.5. Intersected targets between network pharmacology prediction and proteomics**

407 Finally, the intersected targets were analyzed using the Venn method. Three proteins,
408 Crb3, Xaf1, and Tspan4, were identified in the network pharmacology prediction, and
409 these were found to be differentially expressed in the Sch-treated vs. model group in
410 the proteomics analysis (Figure 6A). The interacting network among the Sch-targets-
411 pathway was then built with Cytoscape 3.7.0 (Figure 6B).
412
413 **4. DISCUSSION**
414 Studies on DN are regarded as crucial and fruitful, considering the high medical costs
415 and cardiovascular deterioration of the population globally [40], and are needed to
416 identify innovative treatment for diabetes [41-43]. Our work showed that Sch reduced
417 blood glucose levels, improved biochemical indexes related to renal function, and
418 alleviated renal damage in DN rats to different degrees, indicating that Sch has
419 therapeutic effects on DN disease (Figure 1 and 2).
420
421 The treatment of DN varies according to different disease stages. Drug treatment,
422 dialysis treatment, and renal transplantation are the main methods to treat DN [44], of
423 which drug treatment is the most common. Hemodialysis can prolong the survival rate
424 of patients, but infection, vascular calcification, injury, and other problems may occur
425 after extended treatment [45]. Renal transplantation brings a heavy economic burden to
426 patients, and it can neither prevent the recurrence of DN nor improve other diabetic
427 complications. Therapeutic drugs include antihyperglycemic, antihypertensive, anti-
428 inflammatory, antioxidant, and antifibrosis drugs, among which hyperglycemia control
429 is the main means of treating DN. Dipeptidyl peptidase 4 (DPP-4) inhibitor is a new
430 type 2 diabetes drug. It has been shown to increase the levels of endogenous glucagon-
431 like peptide-1 (GLP-1) and glucose-dependent insulin-stimulating polypeptide (GIP).
432 DPP-4 inhibitors promote pancreatic islet β cell insulin release and inhibit islet α cell
433 glucagon secretion to increase insulin levels and reduce blood sugar. Matsui et al.
434 reported that DPP-4 inhibitors blocked the level of (advanced glycation end products)
435 AGEs and their receptors, reduced proteinuria, and reduced the degree of oxidative

stress in a diabetic rat model [46]. Furthermore, Malek et al. showed that antagonists of the renin-angiotensin system (RAS) regulated renal hemodynamics, mainly through angiotensin II. RAS antagonists have the effects of lowering blood pressure, reducing urinary protein, and delaying the progression of DN disease [47]. Both Yoon et al. and Kang et al. found that angiotensin II induced selective changes in the glomerular basement membrane, increased proteinuria, produced oxidative stress through NADPH oxidase, and activated NF-κB, monocyte chemotactic protein-1 (MCP-1), and transforming growth factor-β (TGF-β) [48, 49]. These proteins were found to promote the generation of inflammation and renal fibrosis and to aggravate damage to the kidney [50]. However, studies have shown that there is a high risk of adverse reactions when such drugs are used [51]. Recently, Kimura et al. showed that sodium glucose cotransporter 2 (SGLT2) inhibitor inhibited the oxidative stress response by inhibiting the TLR signaling pathway, thereby alleviating renal damage in diabetic rats [52]. However, Wang et al. reported that although SGLT2 inhibitors reduced the incidence of hypoglycemia and acute renal injury in patients with type 2 diabetes, they carried a risk of urinary tract infections [53].

Nature is the most generous sponsor of drug research by providing abundant natural bioactive compounds, one of which is Sch. It is a non-enzymatic compound with low toxicity and low cost, and it is a multi-functional traditional medicine, and as such, it has an appealing drug prospect. Sch is a phenylcyclooctene lignan found at high levels in the fruit of *Schisandra chinensis*, a *Magnoliaceae* plant. It improves kidney function and has anti-inflammatory, antioxidant, antitumor, and other pharmacological effects. Lin et al. reported that Sch repressed the expression of Hsp27, downregulated inflammatory cytokines, and inhibited the occurrence of the inflammatory cascade reaction caused by p65 translocation to the nucleus [54]. Feng et al. showed that Sch was metabolized by the cytochrome P450 (CYP450s) enzyme to produce a carbonene active metabolite with the ability to modify peptides in human and mouse liver microsomes, which combined with Keap1 to activate the Nrf2 pathway to reduce liver

damage [55]. Liu et al. showed that Sch activated NF-κB signal transduction, induced the expression of the antiapoptotic protein Survivin, and improved renal function damage caused by cisplatin, thus expanding the clinical application value of cisplatin [56]. Lai et al. found that Sch prevented the accumulation of reactive oxygen species by inhibiting oxidative stress, cell apoptosis, and autophagy and reduced the nephrotoxicity of the immunosuppressant cyclosporine A [57]. Whether Sch inhibits the pathogenesis of DN by regulating antioxidant pathways needs further verification.

Pessoa et al. showed that hyperglycemia caused chronic inflammation in vivo and promoted inflammatory cells to infiltrate into renal tissues, producing pro-inflammatory factors such as IL-1β, IL6, and TNF-α [58]. The release of these inflammatory factors further damaged the mesangial cells and epithelial cells, as well as the renal interstitium, and aggravated proteinuria. Toda et al. found that the levels of inflammatory factors were positively related to the severity of DN [59]. The high-dose Sch group had the most apparent effect on improving renal function, restoring pathological damage of renal tissues, and inhibiting inflammatory reactions in DN rats (Figure 3). These results showed that treatment with Sch had a significant anti-inflammatory effect on the kidneys of DN rats.

The proteomics analysis showed that proteins involved in MAPK signaling and the NF-κB signaling pathway were clustered in the Sch-treated DN rats. The MAPK signaling pathway regulates cell growth, differentiation, environmental stress adaptation, and inflammatory responses. Ran et al. reported that Sch prevented cartilage degeneration in a rat osteoarthritis model through inhibiting MAPK activation by reducing the expression level of p38, extracellular signal-regulated kinase, and c-Jun amino-terminal kinase phosphorylation [60]. Kim et al. also found that MAPK and TGF-β had different effects on the mesangial matrix compared to mesangial cells, resulting in glomerular hypertrophy in the progression of DN [61]. Liu et al. reported that metadherin induced podocyte apoptosis by activating the p38 MAPK-dependent pathway [62]. Furthermore,

Sun et al. showed that the phosphorylation and acetylation levels of NF-κB p65 and signal transducer and activator of transcription 3 (Stat3) were upregulated during DN [63]. Whether Sch affects the epigenetic modification of NF-κB p65 and other proteins involved in MAPK and NF-κB signaling pathway needs further verification. For the prediction of direct interactions of small molecule compounds with target proteins, Almeida et al. isolated a mixture of flavonoids quercetin 3-O-methyl ether (1) and 6-C-methyl quercetin 3-O-methyl ether (2) from the ethyl acetate extract of aerial parts from Vellozia dasypus Seub And they studied the interaction of these two compounds with myeloperoxidase (MPO) by molecular docking [64]. Alves et al. used molecular modeling methods to predict the Raman spectroscopy, IR, and NMR data of piperine alkaloid crystals isolated from pepper (Piper nigrum L.) and compared the calculated data with the experimental data [65]. In future work, we will apply these methods for the prediction of this interaction, and the related validation work.

Tight junctions are cell-cell adhesions in epithelial and endothelial cellular sheets, acting as a primary barrier against the diffusion of solutes through the intracellular space (Figures 4 and 5). It creates a boundary between the apical and the basolateral plasma membrane domains and recruits various cytoskeletal and signaling molecules to their cytoplasmic surface [66]. As identified by our proteomics analysis, the following proteins might have roles in this process: tubulin alpha chain-like 3 (Tubal3), proliferating cell nuclear antigen (Pcna), and Crumbs protein homolog 3 (Crb3). We speculated that Sch may help the kidney create a boundary between the apical and the basolateral plasma membrane and recruit cytoskeletal and signaling molecules at the cytoplasmic surface of certain types of kidney cells.

Among the six possible targets of Sch in treating DN disease, Xaf1 was inhibited in the model vs. control group and induced in the Sch-treated vs. model group. Xaf1 is a negative regulator and its low expression level promoted autophagic cell death [67]. Xaf1 was downregulated in the model vs. control group and upregulated in the Sch-

treated vs. model group (Supplemental Tables S2 and S4). This indicated that Sch may target Xaf1 and increase the expression of Xaf1 to reduce autophagy-related cell death during DN progression, to protect the kidneys of DN patients from damage. Tspan4 was induced in the model vs. control group and reduced in the Sch-treated vs. model group (Supplemental Tables S2 and S4). Ma et al. reported that Tspan4 was a novel histamine H4 receptor (H4R) interactor. H4R is a G protein-coupled receptor mainly expressed on immune cells. When phosphorylated by GPCR kinase, H4R activates G protein and recruits β-arrestins to induce cellular signals in response to agonist stimulation. H4R is considered a key drug target for various inflammatory disorders [68]. We hypothesized that Sch inhibited the inflammation response by inhibiting the expression of Tspan4 and interrupted the interaction between H4R and Tspan4. Zfp512 was reported to be associated with fat deposition and fat biosynthesis in pig muscles [69]. The inhibitory effect of Sch may reduce fat deposition and fat biosynthesis caused by diabetes. Tmigd1 has been shown to protect renal epithelial cells from injury induced by oxidative stress [70]. The suppression of Tmigd1 may be a feedback mechanism based on the induction of SOD or GSH-Px expression levels, or on the inhibition of MDA. Combined with the network pharmacology analysis, the intersected proteins, Crb3, Xaf1, and Tspan4, had the most potential to be Sch targets (Figure 6). The direct interaction between Sch and Crb3/Xaf1/Tspan4 will be verified in subsequent studies.

5. CONCLUSION

In summary, to investigate the possible mechanisms of Sch in treating DN, network pharmacology prediction and quantitative proteomics analysis showed that Sch treats DN by regulating the expression levels of Crb3, Xaf1 and Tspan4 to alleviate oxidative stress and inflammatory responses. These findings provide theoretical basis for elucidating the molecular mechanisms of Sch in treating DN.

ETHICS APPROVAL AND CONSENT TO PARTICIPATE

The experiment was approved by the Ethics Committee of Tianjin University. Approval

No. TJUE-2022-009

HUMAN AND ANIMAL RIGHTS

No humans were used in this study. All animal research procedures were followed in accordance with the standards set forth in the eighth edition of Guide for the Care and Use of Laboratory Animals (published by the National Academy of Sciences, The National Academies Press, Washington, D.C.).

CONSENT FOR PUBLICATION

Not applicable.

FUNDING

This work was financially supported by National Nature Science Foundation of China (grant no. 62061160369).

AVAILABILITY OF DATA AND MATERIALS

Not applicable.

CONFLICT OF INTEREST

None.

ACKNOWLEDGEMENTS

We want to express our sincere gratitude to the laboratory partners who have patiently accompanied the entire writing and organizing process. We thank LetPub for its linguistic assistance during the preparation of this manuscript.

AUTHOR CONTRIBUTIONS

Jianying Song: data analysis, visualization;

Bo Zhang: Funding acquisition;

Xudong Lyu: Writing-original draft;

Huiping Zhang: Data analysis;

Wenbo Cheng: Data analysis; writing-original draft;

Peiyuan Liu: Data analysis; writing-original draft;

Jun Kang: Conceptualization; writing-original draft; funding acquisition; supervision; writing-review and editing.

SUPPLEMENTARY MATERIAL

Supplementary material is available on the publisher's website along with the published article.

REFERENCES

[1] Goldberg, R.; Rubinstein, A.M.; Gil, N.; Hermano, E.; Li, J.P.; van der Vlag, J.; Atzmon, R.; Meirovitz, A.; Elkin, M. Role of heparanase-driven inflammatory cascade in pathogenesis of diabetic nephropathy. *Diabetes*, **2014**, *63*(12), 4302-4313.
[https://doi.org/10.2337/db14-0001] [PMID: 25008182]

[2] Ni, W.J.; Tang, L.Q.; Wei, W. Research progress in signalling pathway in diabetic nephropathy. *Diabetes Metab Res Rev*, **2015**, *31*(3), 221-233.
[https://doi.org/10.1002/dmrr.2568] [PMID: 24898554]

[3] Wang, H.; Zhang, H.; Chen, X.; Zhao, T.; Kong, Q.; Yan, M.; Zhang, B.; Sun, S.; Lan, H.Y.; Li, N.; Li, P. The decreased expression of electron transfer flavoprotein β is associated with tubular cell apoptosis in diabetic nephropathy. *Int J Mol Med*, **2016**, *37*(5), 1290-1298.
[https://doi.org/10.3892/ijmm.2016.2533] [PMID: 27035869]

[4] Jin, H.; Piao, S.G.; Jin, J.Z.; Jin, Y.S.; Cui, Z.H.; Jin, H.F.; Zheng, H.L.; Li, J.J.; Jiang, Y.J.; Yang, C.W.; Li, C. Synergistic effects of leflunomide and benazepril in streptozotocin-induced diabetic nephropathy. *Nephron Exp Nephrol*, **2014**, *126*(3), 148-156.
[https://doi.org/10.1159/000362556] [PMID: 24855017]

[5] Tuttle, K.R.; Bakris, G.L.; Toto, R.D.; McGill, J.B.; Hu, K.; Anderson, P.W. The effect of ruboxistaurin on nephropathy in type 2 diabetes. *Diabetes Care*, **2005**, *28*(11), 2686-2690.
[https://doi.org/10.2337/diacare.28.11.2686] [PMID: 16249540]

[6] Hu, X.; Liu, W.; Yan, Y.; Liu, H.; Huang, Q.; Xiao, Y.; Gong, Z.; Du, J. Vitamin D protects against diabetic nephropathy: Evidence-based effectiveness and mechanism. *Eur J Pharmacol*, **2019**, *845*, 91-98.
[https://doi.org/10.1016/j.ejphar.2018.09.037] [PMID: 30287151]

[7] Tuttle, K.R.; Brosius, F.C., 3rd; Adler, S.G.; Kretzler, M.; Mehta, R.L.; Tumlin, J.A.; Tanaka, Y.; Haneda, M.; Liu, J.; Silk, M.E.; Cardillo, T.E.; Duffin, K.L.; Haas, J.V.; Macias, W.L.; Nunes, F.P.; Janes, J.M. JAK1/JAK2 inhibition by baricitinib in diabetic kidney disease: results from a Phase 2 randomized controlled clinical trial. *Nephrol Dial Transplant*, **2018**, *33*(11), 1950-1959.
[https://doi.org/10.1093/ndt/gfx377] [PMID: 29481660]

[8] Mora, C.; Navarro, J.F. Inflammation and diabetic nephropathy. *Curr Diab Rep*, **2006**, *6*(6), 463-468.
[https://doi.org/10.1007/s11892-006-0080-1] [PMID: 17118230]

[9] Araújo, L.; Silva, M.; Silva, C.; Monteiro, M.; Pereira, L.; Rocha, L.P.; Corrêa, R.; Reis, M.A.; Machado, J.R. Cytokines and T Helper Cells in Diabetic Nephropathy Pathogenesis. **2016**, *6*(6), 230-246.

[10] Wada, J.; Makino, H. Inflammation and the pathogenesis of diabetic nephropathy. *Clin Sci (Lond)*, **2013**, *124*(3), 139-152.

[https://doi.org/10.1042/cs20120198] [PMID: 23075333]
[11] Lampropoulou, I.T.; Stangou, M.; Sarafidis, P.; Gouliovaki, A.; Giamalis, P.; Tsouchnikas, I.; Didangelos, T.; Papagianni, A. TNF-α pathway and T-cell immunity are activated early during the development of diabetic nephropathy in Type II Diabetes Mellitus. *Clin Immunol*, **2020**, *215*, 108423. [https://doi.org/10.1016/j.clim.2020.108423] [PMID: 32304735]
[12] Navarro-González, J.F.; Mora-Fernández, C. The role of inflammatory cytokines in diabetic nephropathy. *J Am Soc Nephrol*, **2008**, *19*(3), 433-442. [https://doi.org/10.1681/asn.2007091048] [PMID: 18256353]
[13] Börgeson, E.; Johnson, A.M.; Lee, Y.S.; Till, A.; Syed, G.H.; Ali-Shah, S.T.; Guiry, P.J.; Dalli, J.; Colas, R.A.; Serhan, C.N.; Sharma, K.; Godson, C. Lipoxin A4 Attenuates Obesity-Induced Adipose Inflammation and Associated Liver and Kidney Disease. *Cell Metab*, **2015**, *22*(1), 125-137. [https://doi.org/10.1016/j.cmet.2015.05.003] [PMID: 26052006]
[14] Liu, W.; Wu, Y.H.; Zhang, L.; Xue, B.; Wang, Y.; Liu, B.; Liu, X.Y.; Zuo, F.; Yang, X.Y.; Chen, F.Y.; Duan, R.; Cai, Y.; Zhang, B.; Ji, Y. MicroRNA-146a suppresses rheumatoid arthritis fibroblast-like synoviocytes proliferation and inflammatory responses by inhibiting the TLR4/NF-kB signaling. *Oncotarget*, **2018**, *9*(35), 23944-23959. [https://doi.org/10.18632/oncotarget.24050] [PMID: 29844864]
[15] Hu, S.; Zuo, H.; Qi, J.; Hu, Y.; Yu, B. Analysis of Effect of Schisandra in the Treatment of Myocardial Infarction Based on Three-Mode Gene Ontology Network. *Front Pharmacol*, **2019**, *10, Article ID 232*. [https://doi.org/10.3389/fphar.2019.00232] [PMID: 30949047]
[16] Thandavarayan, R.A.; Giridharan, V.V.; Arumugam, S.; Suzuki, K.; Ko, K.M.; Krishnamurthy, P.; Watanabe, K.; Konishi, T. Schisandrin B prevents doxorubicin induced cardiac dysfunction by modulation of DNA damage, oxidative stress and inflammation through inhibition of MAPK/p53 signaling. *PLoS One*, **2015**, *10*(3), e0119214. [https://doi.org/10.1371/journal.pone.0119214] [PMID: 25742619]
[17] Xu, Y.; Liu, Z.; Sun, J.; Pan, Q.; Sun, F.; Yan, Z.; Hu, X. Schisandrin B prevents doxorubicin-induced chronic cardiotoxicity and enhances its anticancer activity in vivo. *PLoS One*, **2011**, *6*(12), e28335. [https://doi.org/10.1371/journal.pone.0028335] [PMID: 22164272]
[18] Lee, T.H.; Jung, C.H.; Lee, D.H. Neuroprotective effects of Schisandrin B against transient focal cerebral ischemia in Sprague-Dawley rats. *Food Chem Toxicol*, **2012**, *50*(12), 4239-4245. [https://doi.org/10.1016/j.fct.2012.08.047] [PMID: 22960133]
[19] Wang, J.W.; Liang, F.Y.; Ouyang, X.S.; Li, P.B.; Pei, Z.; Su, W.W. Evaluation of neuroactive effects of ethanol extract of Schisandra chinensis, Schisandrin, and Schisandrin B and determination of underlying mechanisms by zebrafish behavioral profiling. *Chin J Nat Med*, **2018**, *16*(12), 916-925. [https://doi.org/10.1016/s1875-5364(18)30133-x] [PMID: 30595216]
[20] Yu, B.; Sheng, D.; Tan, Q. Determination of Schisandrin A and Schisandrin B in

Traditional Chinese Medicine Preparation Huganpian Tablet by RP-HPLC. *Chem Pharm Bull (Tokyo)*, **2019**, *67*(7), 713-716. [https://doi.org/10.1248/cpb.c18-00968] [PMID: 31006725]

[21] Qin, J.H.; Lin, J.R.; Ding, W.F.; Wu, W.H. Schisandrin B Improves the Renal Function of IgA Nephropathy Rats Through Inhibition of the NF-κB Signalling Pathway. *Inflammation*, **2019**, *42*(3), 884-894. [https://doi.org/10.1007/s10753-018-0943-z] [PMID: 30519926]

[22] Xu, J.; Lu, C.; Liu, Z.; Zhang, P.; Guo, H.; Wang, T. Schizandrin B protects LPS-induced sepsis via TLR4/NF-κB/MyD88 signaling pathway. *Am J Transl Res*, **2018**, *10*(4), 1155-1163. [PMID: 29736208]

[23] Li, M.; Jin, J.; Li, J.; Guan, C.W.; Wang, W.W.; Qiu, Y.W.; Huang, Z.Y. [Schisandrin B protects against nephrotoxicity induced by cisplatin in HK-2 cells via Nrf2-ARE activation]. *Yao Xue Xue Bao*, **2012**, *47*(11), 1434-1439. [PMID: 23387073]

[24] Mou, Z.; Feng, Z.; Xu, Z.; Zhuang, F.; Zheng, X.; Li, X.; Qian, J.; Liang, G. Schisandrin B alleviates diabetic nephropathy through suppressing excessive inflammation and oxidative stress. *Biochem Biophys Res Commun*, **2019**, *508*(1), 243-249. [https://doi.org/10.1016/j.bbrc.2018.11.128] [PMID: 30477745]

[25] Zhou, W.; Zhang, H.; Wang, X.; Kang, J.; Guo, W.; Zhou, L.; Liu, H.; Wang, M.; Jia, R.; Du, X.; Wang, W.; Zhang, B.; Li, S. Network pharmacology to unveil the mechanism of Moluodan in the treatment of chronic atrophic gastritis. *Phytomedicine*, **2022**, *95*, 153837. [https://doi.org/10.1016/j.phymed.2021.153837] [PMID: 34883416]

[26] 张彦琼等. 网络药理学与中医药现代研究的若干进展. *中国药理学与毒理学杂志*, **2015**, *29* (6):883-892.

[27] Li, S.; Zhang, B. Traditional Chinese medicine network pharmacology: theory, methodology and application. *Chin J Nat Med*, **2013**, *11*(2), 110-120. [https://doi.org/10.1016/s1875-5364(13)60037-0] [PMID: 23787177]

[28] Li, S. Mapping ancient remedies: Applying a network approach to traditional Chinese medicine. *Science*, **2015**, *350*(6262), S72-S74.

[29] Zhang, B.; Lu, C.; Bai, M.; He, X.; Tan, Y.; Bian, Y.; Xiao, C.; Zhang, G.; Lu, A.; Li, S. Tetramethylpyrazine identified by a network pharmacology approach ameliorates methotrexate-induced oxidative organ injury. *J Ethnopharmacol*, **2015**, *175*, 638-647. [https://doi.org/10.1016/j.jep.2015.09.034] [PMID: 26435225]

[30] Zhang, B.; Wang, X.; Li, Y.; Wu, M.; Wang, S.Y.; Li, S. Matrine Is Identified as a Novel Macropinocytosis Inducer by a Network Target Approach. *Front Pharmacol*, **2018**, *9*, 10. [https://doi.org/10.3389/fphar.2018.00010] [PMID: 29434546]

[31] Zhang, S.; Lai, X.; Wang, X.; Liu, G.; Wang, Z.; Cao, L.; Zhang, X.; Xiao, W.; Li,

S. Deciphering the Pharmacological Mechanisms of Guizhi-Fuling Capsule on Primary Dysmenorrhea Through Network Pharmacology. *Front Pharmacol*, **2021**, *12*, 613104.
[https://doi.org/10.3389/fphar.2021.613104] [PMID: 33746752]

[32] Guo, Y.; Bao, C.; Ma, D.; Cao, Y.; Li, Y.; Xie, Z.; Li, S. Network-Based Combinatorial CRISPR-Cas9 Screens Identify Synergistic Modules in Human Cells. *ACS Synth Biol*, **2019**, *8*(3), 482-490.
[https://doi.org/10.1021/acssynbio.8b00237] [PMID: 30762338]

[33] Lei, Y.; Li, S.; Liu, Z.; Wan, F.; Tian, T.; Li, S.; Zhao, D.; Zeng, J. A deep-learning framework for multi-level peptide-protein interaction prediction. *Nat Commun*, **2021**, *12*(1), 5465.
[https://doi.org/10.1038/s41467-021-25772-4] [PMID: 34526500]

[34] Zhou, W.; Lai, X.; Wang, X.; Yao, X.; Wang, W.; Li, S. Network pharmacology to explore the anti-inflammatory mechanism of Xuebijing in the treatment of sepsis. *Phytomedicine*, **2021**, *85*, 153543.
[https://doi.org/10.1016/j.phymed.2021.153543] [PMID: 33799226]

[35] Zuo, J.; Wang, X.; Liu, Y.; Ye, J.; Liu, Q.; Li, Y.; Li, S. Integrating Network Pharmacology and Metabolomics Study on Anti-rheumatic Mechanisms and Antagonistic Effects Against Methotrexate-Induced Toxicity of Qing-Luo-Yin. *Front Pharmacol*, **2018**, *9*, 1472.
[https://doi.org/10.3389/fphar.2018.01472] [PMID: 30618762]

[36] Azushima, K.; Gurley, S.B.; Coffman, T.M. Modelling diabetic nephropathy in mice. *Nat Rev Nephrol*, **2018**, *14*(1), 48-56.
[https://doi.org/10.1038/nrneph.2017.142] [PMID: 29062142]

[37] Ge, J.; Miao, J.J.; Sun, X.Y.; Yu, J.Y. Huangkui capsule, an extract from Abelmoschus manihot (L.) medic, improves diabetic nephropathy via activating peroxisome proliferator-activated receptor (PPAR)-α/γ and attenuating endoplasmic reticulum stress in rats. *J Ethnopharmacol*, **2016**, *189*, 238-249.
[https://doi.org/10.1016/j.jep.2016.05.033] [PMID: 27224243]

[38] Wiśniewski, J.R.; Zougman, A.; Nagaraj, N.; Mann, M. Universal sample preparation method for proteome analysis. *Nat Methods*, **2009**, *6*(5), 359-362.
[https://doi.org/10.1038/nmeth.1322] [PMID: 19377485]

[39] Li, S.; Chen, Y.T.; Ding, Q.Y.; Dai, J.Y.; Duan, X.C.; Hu, Y.J.; Lai, X.X.; Liu, Q.F.; Niu, M.; Xiang, R.W. Network Pharmacology Evaluation Method Guidance-Draft. *WJTCM*, **2021**, *7*(1), 146-154.

[40] Meza Letelier, C.E.; San Martín Ojeda, C.A.; Ruiz Provoste, J.J.; Frugone Zaror, C.J. [Pathophysiology of diabetic nephropathy: a literature review]. *Medwave*, **2017**, *17*(1), e6839
[https://doi.org/10.5867/medwave.2017.01.6839] [PMID: 28112712]

[41] Gao, H.; Wu, H. Maslinic acid activates renal AMPK/SIRT1 signaling pathway and protects against diabetic nephropathy in mice. *BMC Endocr Disord*, **2022**, *22*(1), 25-35.
[https://doi.org/10.1186/s12902-022-00935-6] [PMID: 35042497]

[42] Carmona, M.; Paco-Meza, L.M.; Ortega, R.; Cañadillas, S.; Caballero-Villarraso,

J.; Blanco, A.; Herrera, C. Hypoxia preconditioning increases the ability of healthy but not diabetic rat-derived adipose stromal/stem cells (ASC) to improve histological lesions of streptozotocin-induced diabetic nephropathy. *Pathol Res Pract*, **2022**, *230, Article ID 153756*. [https://doi.org/10.1016/j.prp.2021.153756] [PMID: 35032832]

[43] Nagib, A.M.; Elsayed Matter, Y.; Gheith, O.A.; Refaie, A.F.; Othman, N.F.; Al-Otaibi, T. Diabetic Nephropathy Following Posttransplant Diabetes Mellitus. *Exp Clin Transplant*, **2019**, *17*(2), 138-146. [https://doi.org/10.6002/ect.2018.0157] [PMID: 30945628]

[44] Selby, N.M.; Taal, M.W. An updated overview of diabetic nephropathy: Diagnosis, prognosis, treatment goals and latest guidelines. *Diabetes Obes Metab*, **2020**, *22*(Suppl 1), 3-15. [https://doi.org/10.1111/dom.14007] [PMID: 32267079]

[45] Markell, M.S.; Friedman, E.A. Diabetic nephropathy. Management of the end-stage patient. *Diabetes Care*, **1992**, *15*(9), 1226-1238. [https://doi.org/10.2337/diacare.15.9.1226] [PMID: 1396019]

[46] Matsui, T.; Nakashima, S.; Nishino, Y.; Ojima, A.; Nakamura, N.; Arima, K.; Fukami, K.; Okuda, S.; Yamagishi, S. Dipeptidyl peptidase-4 deficiency protects against experimental diabetic nephropathy partly by blocking the advanced glycation end products-receptor axis. *Lab Invest*, **2015**, *95*(5), 525-533. [https://doi.org/10.1038/labinvest.2015.35] [PMID: 25730373]

[47] Malek, V.; Sharma, N.; Sankrityayan, H.; Gaikwad, A.B. Concurrent neprilysin inhibition and renin-angiotensin system modulations prevented diabetic nephropathy. *Life Sci*, **2019**, *221*, 159-167. [https://doi.org/10.1016/j.lfs.2019.02.027] [PMID: 30769114]

[48] Yoon, J.J.; Park, J.H.; Kim, H.J.; Jin, H.G.; Kim, H.Y.; Ahn, Y.M.; Kim, Y.C.; Lee, H.S.; Lee, Y.J.; Kang, D.G. Dianthus superbus Improves Glomerular Fibrosis and Renal Dysfunction in Diabetic Nephropathy Model. *Nutrients*, **2019**, *11*(3), 553-571. [https://doi.org/10.3390/nu11030553] [PMID: 30841605]

[49] Kang, J.S.; Lee, S.J.; Lee, J.H.; Kim, J.H.; Son, S.S.; Cha, S.K.; Lee, E.S.; Chung, C.H.; Lee, E.Y. Angiotensin II-mediated MYH9 downregulation causes structural and functional podocyte injury in diabetic kidney disease. *Sci Rep*, **2019**, *9*(1), 7679-7691. [https://doi.org/10.1038/s41598-019-44194-3] [PMID: 31118506]

[50] Ruggenenti, P.; Cravedi, P.; Remuzzi, G. The RAAS in the pathogenesis and treatment of diabetic nephropathy. *Nat Rev Nephrol*, **2010**, *6*(6), 319-330. [https://doi.org/10.1038/nrneph.2010.58] [PMID: 20440277]

[51] Harel, Z.; Gilbert, C.; Wald, R.; Bell, C.; Perl, J.; Juurlink, D.; Beyene, J.; Shah, P.S. The effect of combination treatment with aliskiren and blockers of the renin-angiotensin system on hyperkalaemia and acute kidney injury: systematic review and meta-analysis. *BMJ*, **2012**, *344, Article ID e42*. [https://doi.org/10.1136/bmj.e42] [PMID: 22232539]

[52] Kimura, Y.; Kuno, A.; Tanno, M.; Sato, T.; Ohno, K.; Shibata, S.; Nakata, K.;

Sugawara, H.; Abe, K.; Igaki, Y.; Yano, T.; Miki, T.; Miura, T. Canagliflozin, a sodium-glucose cotransporter 2 inhibitor, normalizes renal susceptibility to type 1 cardiorenal syndrome through reduction of renal oxidative stress in diabetic rats. *J Diabetes Investig*, **2019**, *10*(4), 933-946. [https://doi.org/10.1111/jdi.13009] [PMID: 30663266]

[53] Wang, M.; Zhang, X.; Ni, T.; Wang, Y.; Wang, X.; Wu, Y.; Zhu, Z.; Li, Q. Comparison of New Oral Hypoglycemic Agents on Risk of Urinary Tract and Genital Infections in Type 2 Diabetes: A Network Meta-analysis. *Adv Ther*, **2021**, *38*(6), 2840-2853. [https://doi.org/10.1007/s12325-021-01759-x] [PMID: 33999339]

[54] Lin, Q.N.; Liu, Y.D.; Guo, S.E.; Zhou, R.; Huang, Q.; Zhang, Z.M.; Qin, X. Schisandrin B ameliorates high-glucose-induced vascular endothelial cells injury by regulating the Noxa/Hsp27/NF-κB signaling pathway. *Biochem Cell Biol*, **2019**, *97*(6), 681-692. [https://doi.org/10.1139/bcb-2018-0321] [PMID: 30817212]

[55] Feng, S.; Qiu, B.; Zou, L.; Liu, K.; Xu, X.; Zhu, H. Schisandrin B elicits the Keap1-Nrf2 defense system via carbene reactive metabolite which is less harmful to mice liver. *Drug Des Devel Ther*, **2018**, *12*, 4033-4046. [https://doi.org/10.2147/dddt.S176561] [PMID: 30568426]

[56] Liu, Q.; Song, J.; Li, H.; Dong, L.; Dai, S. Schizandrin B inhibits the cis-DDP-induced apoptosis of HK-2 cells by activating ERK/NF-κB signaling to regulate the expression of survivin. *Int J Mol Med*, **2018**, *41*(4), 2108-2116. [https://doi.org/10.3892/ijmm.2018.3409] [PMID: 29393335]

[57] Lai, Q.; Luo, Z.; Wu, C.; Lai, S.; Wei, H.; Li, T.; Wang, Q.; Yu, Y. Attenuation of cyclosporine A induced nephrotoxicity by schisandrin B through suppression of oxidative stress, apoptosis and autophagy. *Int Immunopharmacol*, **2017**, *52*, 15-23. [https://doi.org/10.1016/j.intimp.2017.08.019] [PMID: 28846887]

[58] Pessoa, E.A.; Convento, M.B.; Castino, B.; Leme, A.M.; de Oliveira, A.S.; Aragão, A.; Fernandes, S.M.; Carbonel, A.; Dezoti, C.; Vattimo, M.F.; Schor, N.; Borges, F.T. Beneficial Effects of Isoflavones in the Kidney of Obese Rats Are Mediated by PPAR-Gamma Expression. *Nutrients*, **2020**, *12*(6), 1624-1643. [https://doi.org/10.3390/nu12061624] [PMID: 32492810]

[59] Toda, N.; Mukoyama, M.; Yanagita, M.; Yokoi, H. CTGF in kidney fibrosis and glomerulonephritis. *Inflamm Regen*, **2018**, *38*, 14-21. [https://doi.org/10.1186/s41232-018-0070-0] [PMID: 30123390]

[60] Ran, J.; Ma, C.; Xu, K.; Xu, L.; He, Y.; Moqbel, S.A.A.; Hu, P.; Jiang, L.; Chen, W.; Bao, J.; Xiong, Y.; Wu, L. Schisandrin B ameliorated chondrocytes inflammation and osteoarthritis via suppression of NF-κB and MAPK signal pathways. *Drug Des Devel Ther*, **2018**, *12*, 1195-1204. [https://doi.org/10.2147/dddt.S162014] [PMID: 29785089]

[61] Kim, N.H. Podocyte hypertrophy in diabetic nephropathy. *Nephrology (Carlton)*, **2005**, *10*, S14-16. [https://doi.org/10.1111/j.1440-1797.2005.00450.x] [PMID: 16174280]

[62] Liu, W.T.; Peng, F.F.; Li, H.Y.; Chen, X.W.; Gong, W.Q.; Chen, W.J.; Chen, Y.H.; Li, P.L.; Li, S.T.; Xu, Z.Z.; Long, H.B. Metadherin facilitates podocyte apoptosis in diabetic nephropathy. *Cell Death Dis*, **2016**, *7*(11), e2477. [https://doi.org/10.1038/cddis.2016.335] [PMID: 27882943]

[63] Sun, H.J.; Xiong, S.P.; Cao, X.; Cao, L.; Zhu, M.Y.; Wu, Z.Y.; Bian, J.S. Polysulfide-mediated sulfhydration of SIRT1 prevents diabetic nephropathy by suppressing phosphorylation and acetylation of p65 NF-κB and STAT3. *Redox Biol*, **2021**, *38*, 101813. [https://doi.org/10.1016/j.redox.2020.101813] [PMID: 33279869]

[64] Almeida, V.M.; Dias Ê, R.; Souza, B.C.; Cruz, J.N.; Santos, C.B.R.; Leite, F.H.A.; Queiroz, R.F.; Branco, A. Methoxylated flavonols from Vellozia dasypus Seub ethyl acetate active myeloperoxidase extract: in vitro and in silico assays. *J Biomol Struct Dyn*, **2022**, *40*(16), 7574-7583. [https://doi.org/10.1080/07391102.2021.1900916] [PMID: 33739225]

[65] Alves, F.S.; Rodrigues Do Rego, J.d.A.; Da Costa, M.L.; Lobato Da Silva, L.F.; Da Costa, R.A.; Cruz, J.N.; Brasil, D.D.S.B. Spectroscopic methods and in silico analyses using density functional theory to characterize and identify piperine alkaloid crystals isolated from pepper (Piper Nigrum L.). *Journal of Biomolecular Structure and Dynamics*, **2020**, *38*(9), 2792-2799. [https://doi.org/10.1080/07391102.2019.1639547]

[66] Tsukita, S. Tight Junctions. *Encyclopedia of Biological Chemistry*, **2013**, 392-395. [https://doi.org/https://doi.org/10.1016/B978-0-12-378630-2.00440-0]

[67] Sun, P.H.; Zhu, L.M.; Qiao, M.M.; Zhang, Y.P.; Jiang, S.H.; Wu, Y.L.; Tu, S.P. The XAF1 tumor suppressor induces autophagic cell death via upregulation of Beclin-1 and inhibition of Akt pathway. *Cancer Lett*, **2011**, *310*(2), 170-180. [https://doi.org/10.1016/j.canlet.2011.06.037] [PMID: 21788101]

[68] Ma, X.; Verweij, E.W.E.; Siderius, M.; Leurs, R.; Vischer, H.F. Identification of TSPAN4 as Novel Histamine H(4) Receptor Interactor. *Biomolecules*, **2021**, *11*(8), 1127-1142. [https://doi.org/10.3390/biom11081127] [PMID: 34439793]

[69] Ma, C.; Wang, W.; Wang, Y.; Sun, Y.; Kang, L.; Zhang, Q.; Jiang, Y. TMT-labeled quantitative proteomic analyses on the longissimus dorsi to identify the proteins underlying intramuscular fat content in pigs. *J Proteomics*, **2020**, *213*, 103630. [https://doi.org/10.1016/j.jprot.2019.103630] [PMID: 31881348]

[70] Wu, Y.; Li, E.; Wang, Z.; Shen, T.; Shen, C.; Liu, D.; Gao, Q.; Li, X.; Wei, G. TMIGD1 Inhibited Abdominal Adhesion Formation by Alleviating Oxidative Stress in the Mitochondria of Peritoneal Mesothelial Cells. *Oxid Med Cell Longev*, **2021**, 9993704. [https://doi.org/10.1155/2021/9993704] [PMID: 34426761]

884 **Figure legends**

885 **Scheme 1.** Schematic diagram of the experimental method flow.

886

887 **Figure 1.** Sch treatment alleviated hyperglycemia and lowered creatinine, blood urea
888 nitrogen, and urine protein in diabetic nephropathy (DN) rats. A. Sch treatment
889 decreased the body weight of DN rats. B. Sch treatment decreased the fasting blood
890 glucose in DN rats. C. Concentration of creatinine was decreased in Sch-treated DN
891 rats. D. Blood urea nitrogen was decreased in Sch-treated DN rats. E. Urine protein was
892 decreased in DN rats after Sch treatment.
893 Negative control, model, positive control, Sch low dose, Sch high dose groups (n = 10
894 per group). Data are presented as the mean ± SD. ##: $P < 0.01$ as compared to the
895 control group; *: $P < 0.05$ as compared to the model group; **: $P < 0.01$ as compared
896 to the model group. ***: $P < 0.001$ as compared to the model group.

897

898 **Figure 2.** Sch treatment significantly improved the pathological changes of the kidneys
899 in DN model rats. A. HE staining of a rat kidney. Bar = 200 μm. B. Masson staining of
900 a rat kidney. Bar = 200 μm. C. Sirius red staining of a rat kidney. Bar = 100 μm.

901

902 **Figure 3.** Sch showed anti-oxidative activity and inhibited the expression of pro-
903 inflammatory cytokines in the serum of DN rats. A–C. SOD level (A) and MDA (B)
904 and GSH-Px concentrations (C) in negative control and DN rats. D. Sch treatment
905 inhibited the levels of pro-inflammatory cytokines in the serum.
906 Negative control, model, positive control, Sch low dose, Sch high dose groups (n = 10
907 per group). Data are presented as the mean ± SD. ##: $P < 0.01$ as compared to the
908 control group; *: $P < 0.05$ as compared to the model group; **: $P < 0.01$ as compared
909 to the model group. ***: $P < 0.001$ as compared to the model group.

910

911 **Figure 4.** Network pharmacology analysis of intersecting genes between Sch targets
912 and DN targets. A. Eleven intersecting genes were identified using Venn analysis. B–

913 D. GO term analysis of the 11 genes, including biological process (B), cell component
914 (C), and molecular function (D). E. KEGG analysis of the 11 genes. F. Bioactive-
915 protein-pathway network of Sch, target genes, and the related pathways. The pink
916 polygon represents Sch, the green rectangle represents the target genes, and the orange
917 oval represents the related pathways.
918
919 **Figure 5.** Quantitative proteomics analysis. A. Venn analysis of the upregulated
920 proteins in the model vs. control group and downregulated proteins in the Sch-treated
921 vs. model group. B. Venn analysis of the downregulated proteins in the model vs.
922 control group and upregulated proteins in the Sch-treated vs. model group. C. Heatmap
923 analysis of the differentially expressed proteins in the Sch-treated vs. model group. E–
924 G. GO term analysis of the differentially expressed proteins in the Sch-treated vs. model
925 group, including biological process (E), cell component (F), and molecular function (G).
926 H. KEGG analysis of the differentially expressed proteins.
927
928 **Figure 6.** Three intersecting genes and the Sch-target-pathway network between the
929 network pharmacology analysis and proteomics analysis. A. Three intersecting genes
930 was identified using Venn analysis. B. Sch-target-pathway network. The pink rectangle
931 represents Sch, the magenta triangles represent targets, and the blue circles represent
932 pathways.
933
934 **Supplemental materials**
935 Supplemental Figure S1. Identified protein and peptide number from the quantitative
936 proteomics.
937 Supplemental Table S1. Intersecting gene list between Schisandrin B target genes and
938 diabetic nephropathy target genes.
939 Supplemental Table S2. Differentially expressed proteins in the model vs. control group.
940 Supplemental Table S3. Differentially expressed proteins in the Sch-treated vs. control
941 group.

942 Supplemental Table S4. Differentially expressed proteins in the Sch-treated vs. model
943 group.

Song et al. Scheme 1

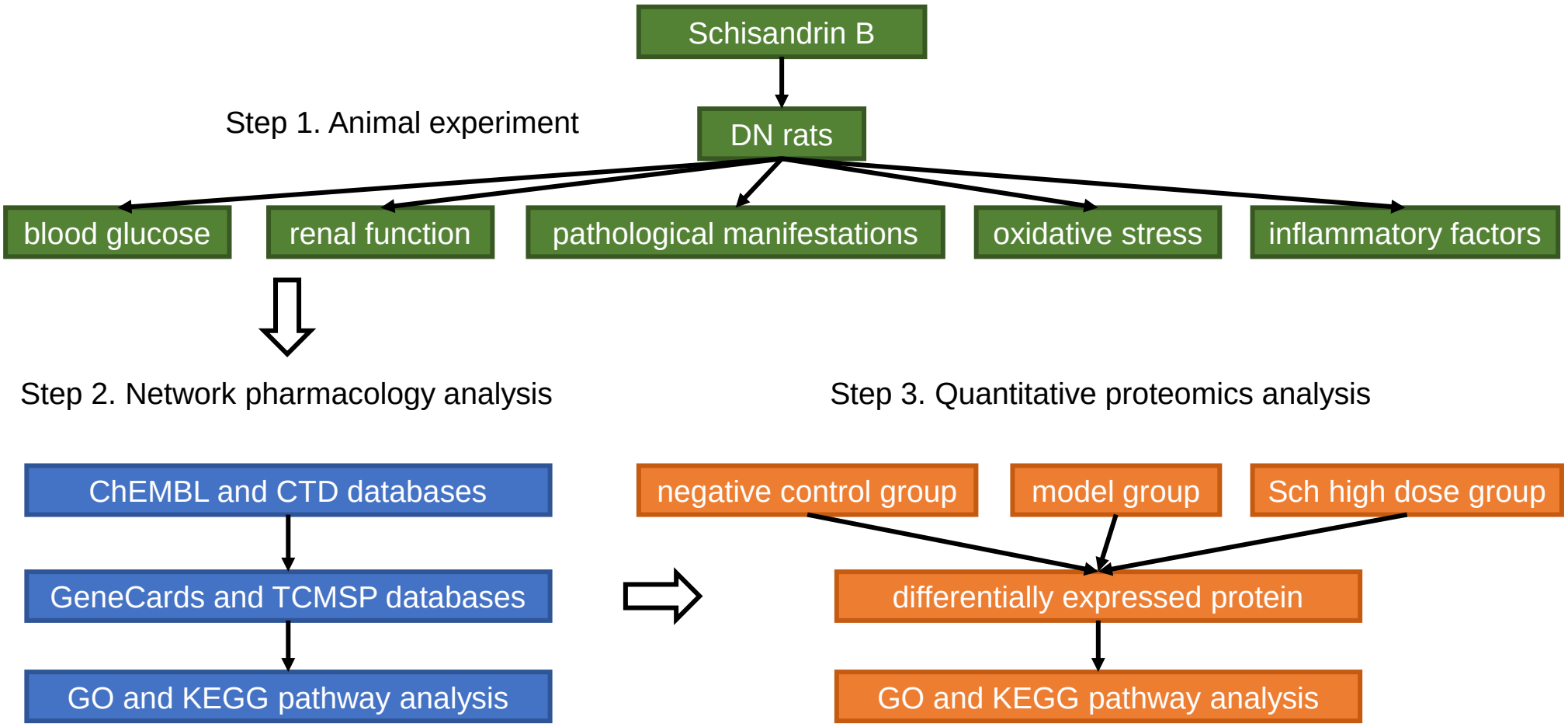

Song et al. Figure 1

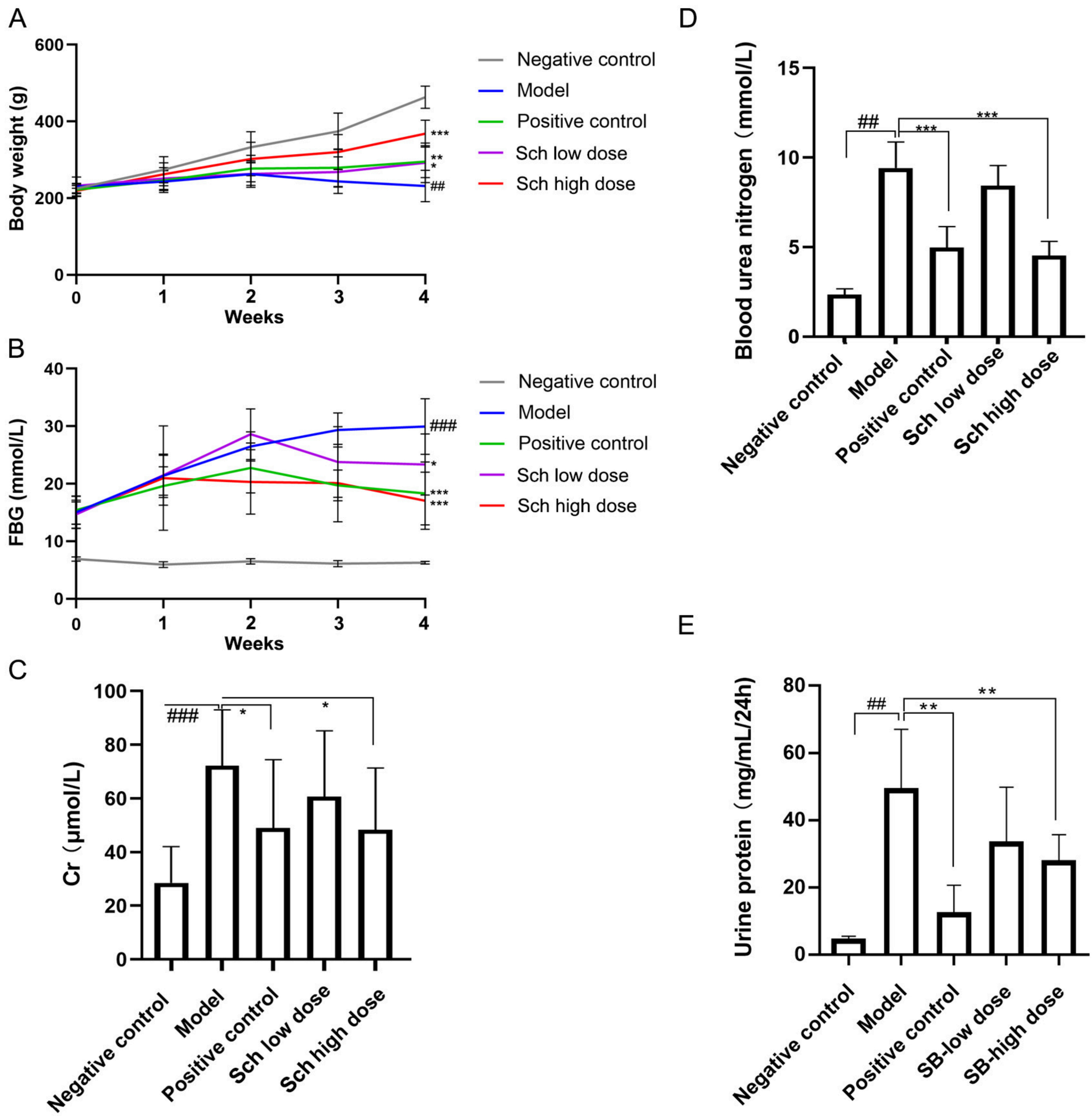

Song et al. Figure 2

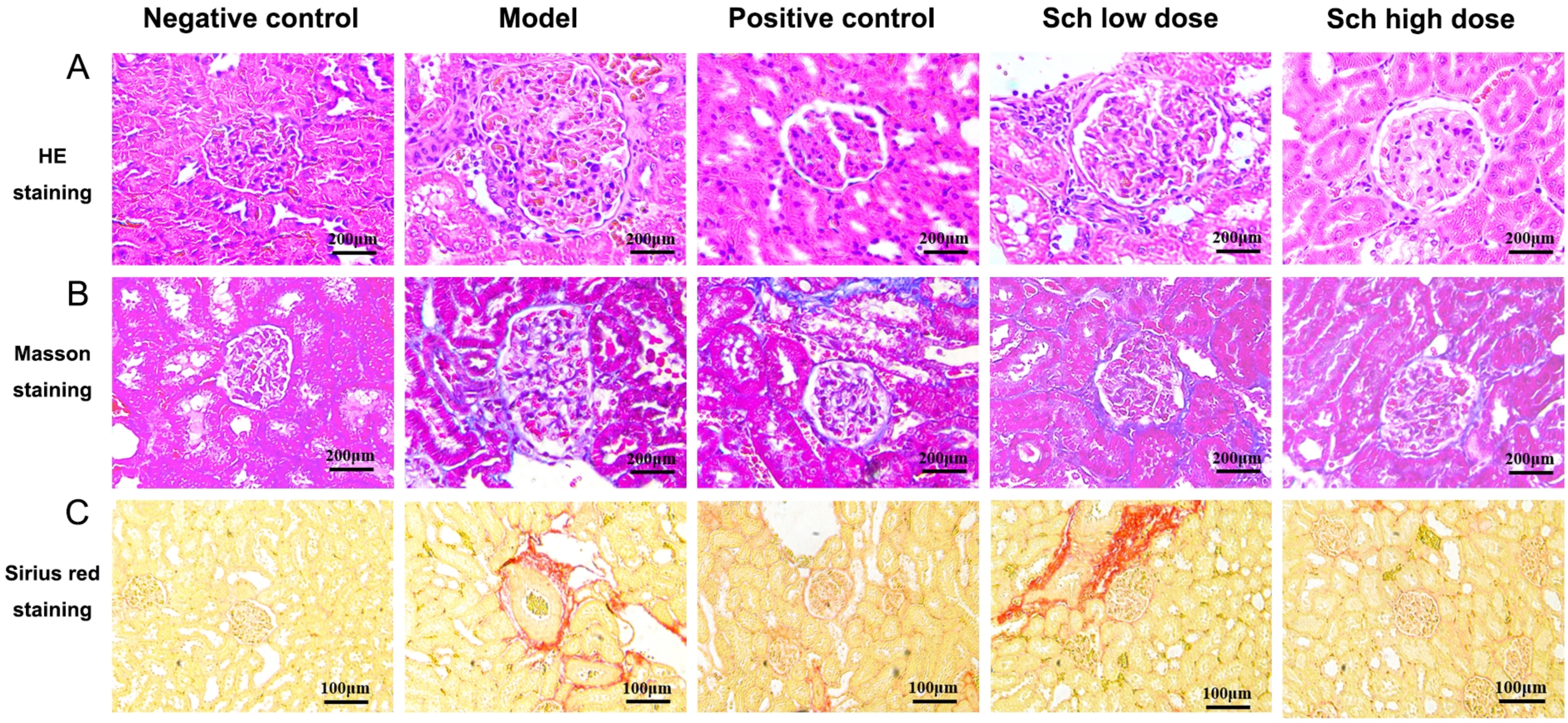

Song et al. Figure 3

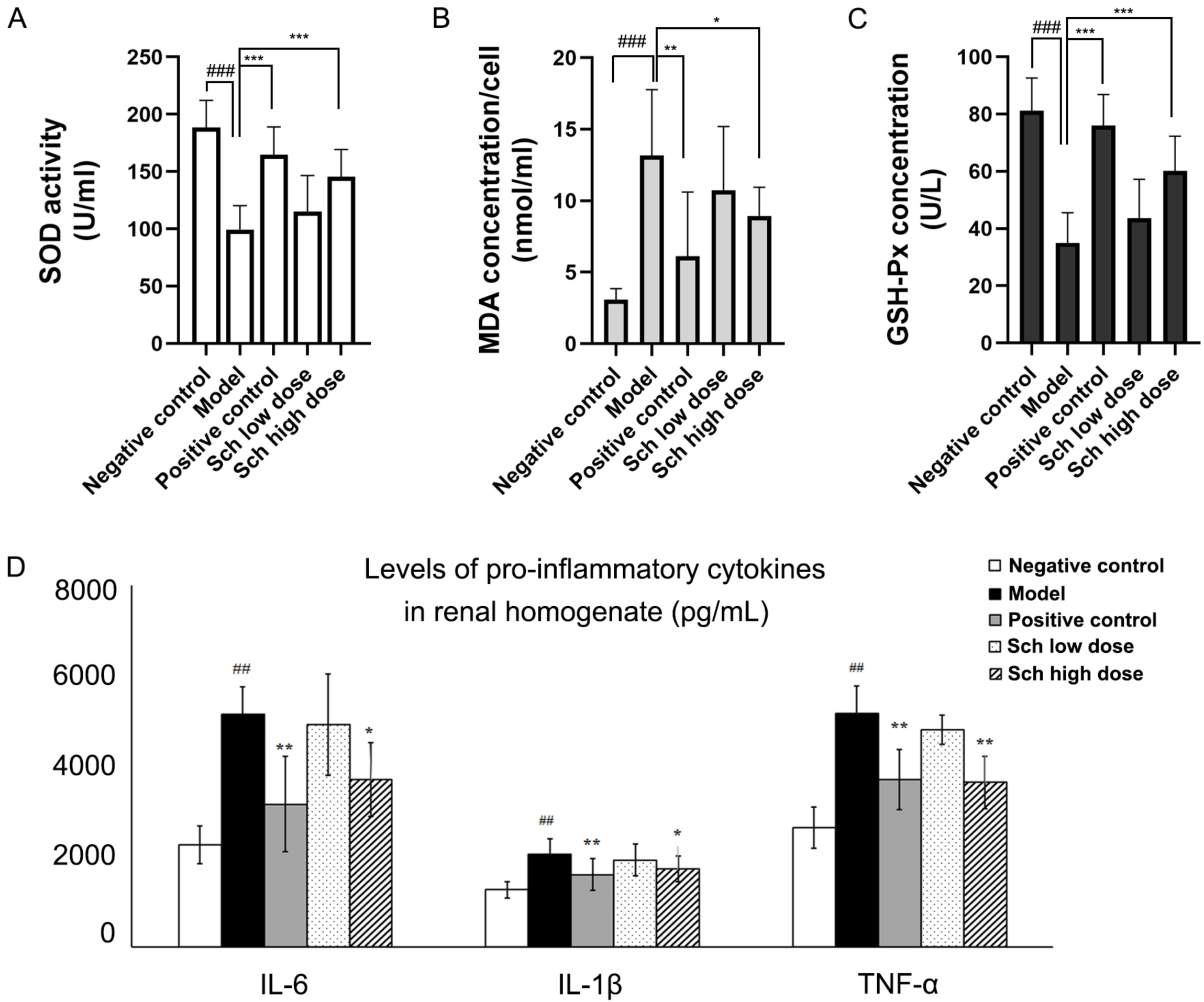

Song et al. Figure 4

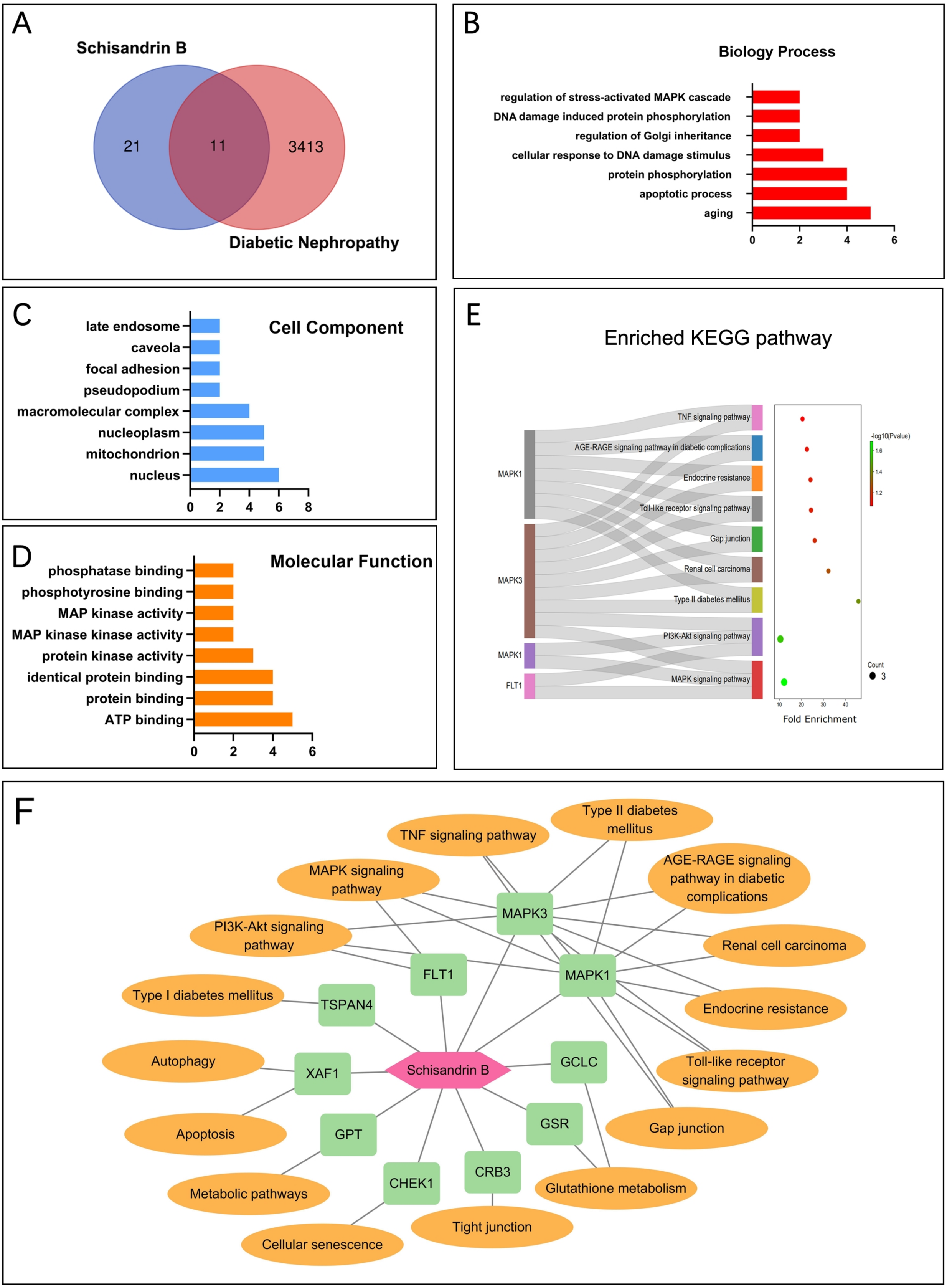

Zhang et al. Figure 5

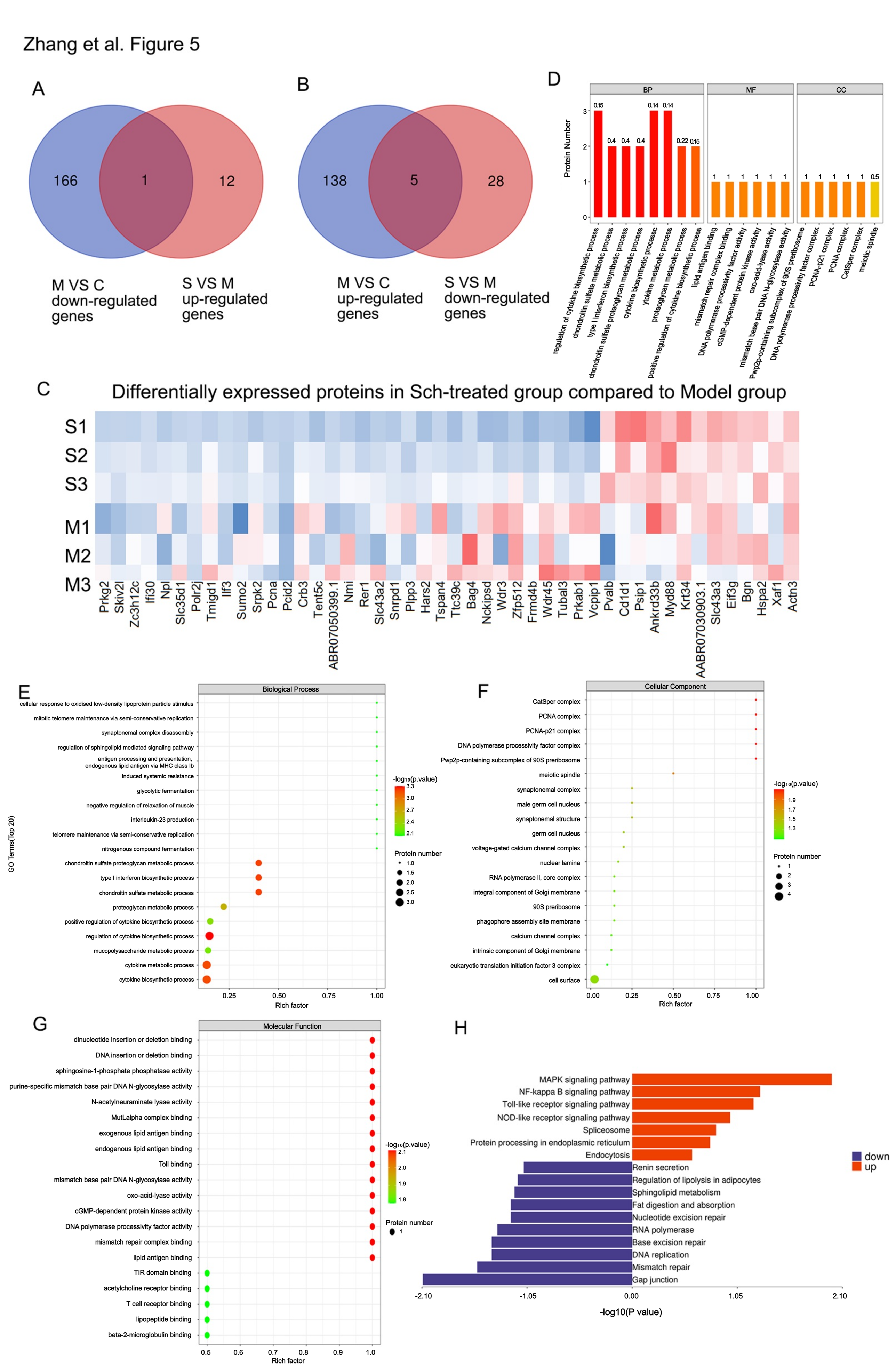

Song et al. Figure 6

A

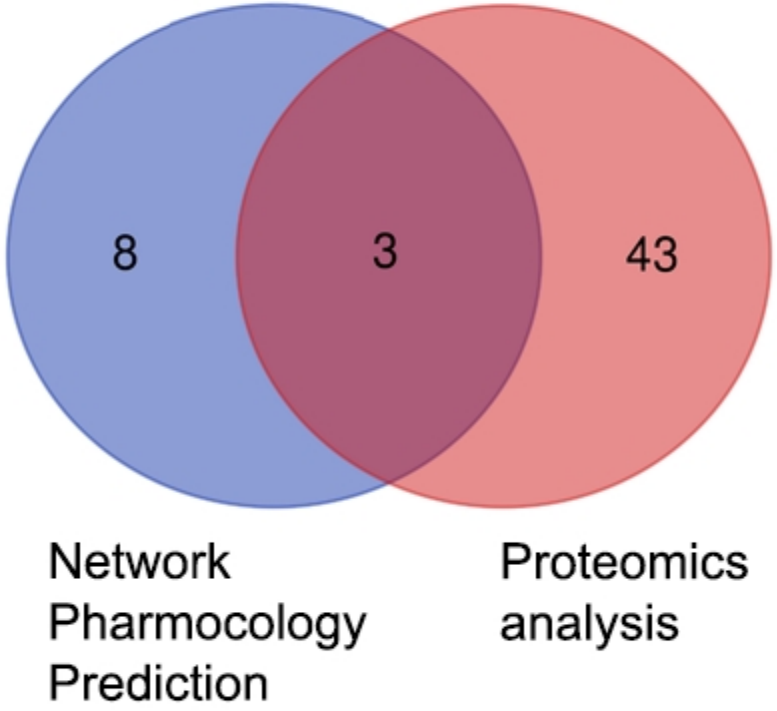
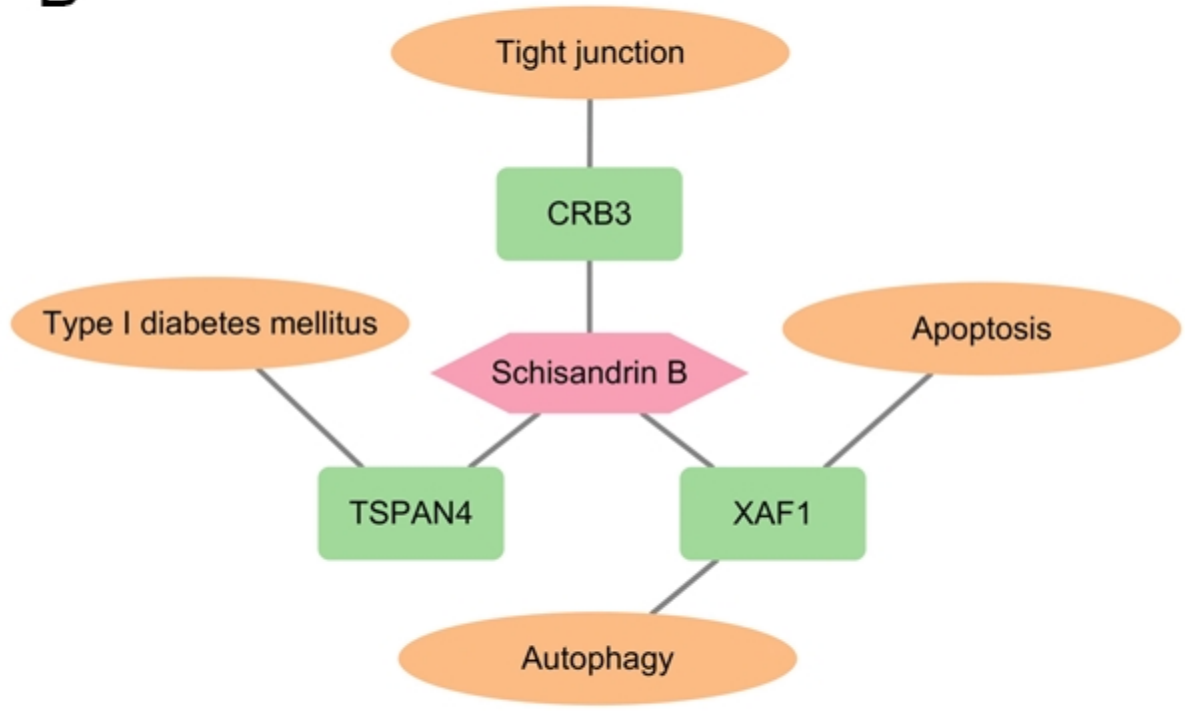
B